

Next-to-leading order QCD predictions for the hadronic WH +jet production

Su Ji-Juan, Ma Wen-Gan, Zhang Ren-You, and Guo Lei

Department of Modern Physics, University of Science and Technology
of China (USTC), Hefei, Anhui 230026, People's Republic of China

Abstract

We calculate the next-to-leading order(NLO) QCD corrections to the WH^0 production in association with a jet at hadron colliders. We study the impacts of the complete NLO QCD radiative corrections to the integrated cross sections, the scale dependence of the cross sections, and the differential cross sections ($\frac{d\sigma}{d\cos\theta}$, $\frac{d\sigma}{dp_T}$) of the final W^- , Higgs boson and jet. We find that the corrections significantly modify the physical observables, and reduce the scale uncertainty of the leading-order cross section. Our results show that by applying the inclusive scheme with $p_{T,j}^{cut} = 20 \text{ GeV}$ and taking $m_H = 120 \text{ GeV}$, $\mu = \mu_0 \equiv \frac{1}{2}(m_W + m_H)$, the K-factor is 1.15 for the process $p\bar{p} \rightarrow W^\pm H^0 j + X$ at the Tevatron, while the K-factors for the processes $pp \rightarrow W^- H^0 j + X$ and $pp \rightarrow W^+ H^0 j + X$ at the LHC are 1.12 and 1.08 respectively. We conclude that to understand the hadronic associated WH^0 production, it is necessary to study the NLO QCD corrections to the $WH^0 j$ production process which is part of the inclusive WH^0 production.

PACS: 12.38.Bx, 13.85.-t, 14.80.Bn, 14.70.Fm

1. Introduction

In the standard model (SM) the Higgs mechanism explains the mass generation, and is believed to be responsible for the breaking of the electroweak (EW) symmetry[1, 2]. To discover the Higgs boson and investigate thoroughly the mechanism of EW symmetry breaking are the main physics motivations for the future high energy colliders. At the Fermilab Tevatron, Higgs boson production associated with the W or Z^0 boson, is the most important discovery channel for the SM Higgs boson with light mass($m_H < 135 \text{ GeV}$)[3, 4]. At the CERN LHC there are a few Higgs boson production mechanisms which lead to an observable cross section. Each of them makes use of the preference of couplings of the SM Higgs and massive gauge bosons or top quarks[5]. Recently, J.M. Butterworth, *et al.* concluded that the subset techniques at the LHC have the potential to transform the high- p_T WH^0 , $Z^0H^0(H^0 \rightarrow b\bar{b})$ channel into one of the best channels in finding a low mass SM Higgs and obtaining the unique information on the coupling of the Higgs boson separately to W and Z^0 bosons[6].

At the TeV energy scale hadron colliders, the experimental environment is extremely complicated. The produced signal and background reactions normally involve multiparticles in the final state. A good understanding of these reactions is very necessary for studying the hadronic collider physics. It requires sufficiently precise predictions for the new physics signals and their backgrounds with multiple final particles which cannot entirely be separated in experimental data. Therefore, high-order predictions for these reactions are very useful. In fact, when we measure experimentally the inclusive WH^0 production signal, it includes any number of additional jets unless stated otherwise. In this sense the WH^0 +jet production is part of the inclusive WH^0 production, and theoretically WH^0 +jet at the next-to-leading order(NLO) QCD is part of the WH^0 production process at the NNLO QCD. Recently, the calculations of the QCD $\mathcal{O}(\alpha_s)$ and electroweak $\mathcal{O}(\alpha_{ew})$ corrections to the Higgs production processes $p\bar{p}/pp \rightarrow WH^0/Z^0H^0 + X$ at the Tevatron and the LHC were presented in Refs. [7, ?], respectively. The NNLO QCD corrections to the SM Higgs boson production processes in association with the vector boson at hadron colliders have been calculated in Ref.[9].

In this work we present precise calculations for the process $p\bar{p}/pp \rightarrow WH^0j + X$ up to the

QCD NLO at the Tevatron and the LHC. The paper is organized as follows: We describe the technical details of the related leading-order(LO) and NLO QCD calculations in Secs. 2 and 3, respectively. In Sec.4 we give some numerical results and discussions about the NLO QCD corrections. Finally a short summary is given.

2. LO cross sections

At the partonic level the cross section for the W^+H^0j production process in the SM should be the same as for the W^-H^0j production process due to the CP-conservation. We present the LO calculations for the related partonic W^-H^0j production processes in this section. We calculate the $p\bar{p}/pp \rightarrow W^\pm H^0j + X$ processes by neglecting u-, d-, c-, s-, b-quark mass($m_u = m_d = m_c = m_s = m_b = 0$), and the quark mixing between the third generation and other two generations(i.e., $V_{ub} = V_{cb} = V_{td} = V_{ts} = 0$). In our LO calculation we do not consider the partonic processes with an incoming (anti)bottom-quark due to the heavy (anti)bottom-quark suppression in parton distribution functions (PDFs) in the proton and antiproton. Then the following partonic processes are involved in our LO calculations.

$$\bar{q}(p_1) + q'(p_2) \rightarrow W^-(p_3) + H^0(p_4) + g(p_5), \quad (2.1)$$

$$\bar{q}(p_1) + g(p_2) \rightarrow W^-(p_3) + H^0(p_4) + \bar{q}'(p_5), \quad (2.2)$$

$$q'(p_1) + g(p_2) \rightarrow W^-(p_3) + H^0(p_4) + q(p_5), \quad (2.3)$$

where $q = u, c$; $q' = d, s$. $p_i(i = 1, \dots, 5)$ represent the four-momenta of the incoming partons and the outgoing W^- , H^0 and jet, respectively. There are six LO Feynman diagrams for all those partonic processes of the W^-H^0j production shown in Fig.1. There Figs.1(a,b), Figs.1(c,d) and Figs.1(e,f) are the LO diagrams for the partonic process $\bar{q}q' \rightarrow W^-H^0g$, $\bar{q}g \rightarrow W^-H^0\bar{q}'$ and $q'g \rightarrow W^-H^0q$, respectively.

All partonic processes for W^-H^0j production at hadron colliders are related to the amplitude $0 \rightarrow W^-H^0q\bar{q}'g$ by crossing symmetry. The expressions of the LO cross sections for the partonic processes $\bar{q}q' \rightarrow W^-H^0g$, $\bar{q}g \rightarrow W^-H^0\bar{q}'$ and $q'g \rightarrow W^-H^0q$ can be written in the

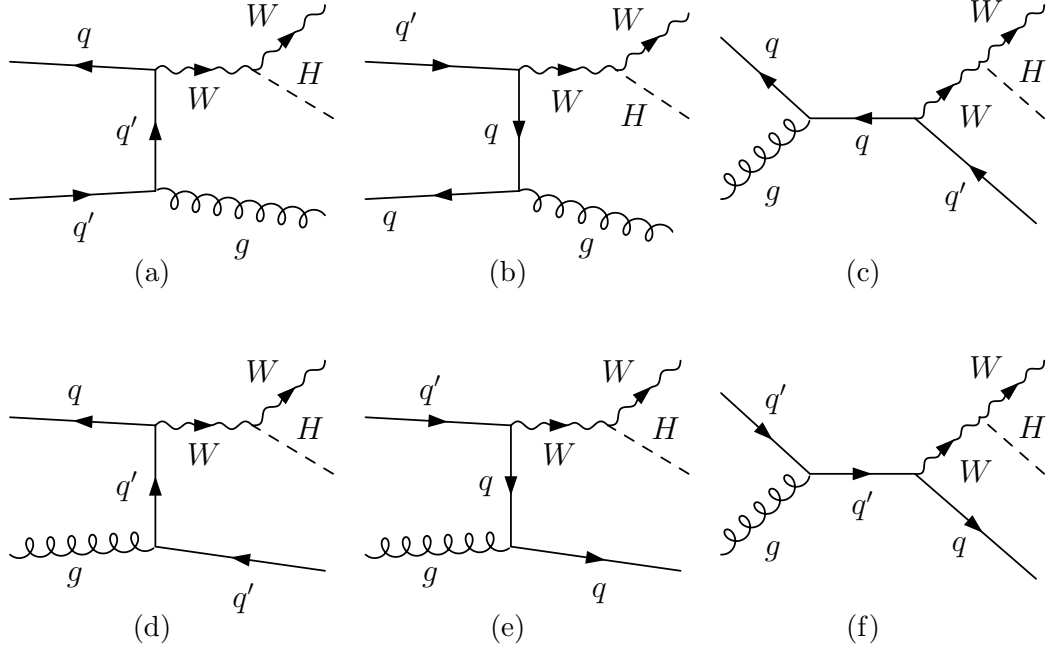


Figure 1: The generic LO Feynman diagrams for the partonic processes $\bar{q}q'(g) \rightarrow W^-H^0g(\bar{q}')$ and $q'g \rightarrow W^-H^0q$. Figures 1 (a) and (b) are the LO diagrams for the partonic process $\bar{q}q' \rightarrow W^-H^0g$, (c) and (d) for the $\bar{q}g \rightarrow W^-H^0q'$, (e) and (f) for the $q'g \rightarrow W^-H^0q$, ($q = u, c$; $q' = d, s$).

form as,

$$\hat{\sigma}_{LO}^{kl}(\hat{s}) = \frac{1}{2\hat{s}} \int \overline{\sum} |\mathcal{M}_{LO}^{kl}|^2 d\Omega_3^{kl}, \quad (kl = \bar{q}q', \bar{q}g, q'g, (q = u, c; q' = d, s)), \quad (2.4)$$

where the summation is taken over the spins and colors of final states, and the bar over the summation recalls averaging over the spin and color degrees of freedom of initial partons. $d\Omega_3^{kl}$ is the three-body phase-space element for the $kl \rightarrow W^-H^0j$ channel expressed as

$$d\Omega_3^{kl} = (2\pi)^4 \delta^4(p_1 + p_2 - \sum_{i=3}^5 p_i) \prod_{j=3}^5 \frac{d^3p_j}{(2\pi)^3 2E_j}. \quad (2.5)$$

In Eq.(2.4) \mathcal{M}_{LO}^{kl} is the amplitude of the tree-level diagrams for any one of the partonic processes (2.1)-(2.3). \hat{s} is the partonic center-of-mass energy squared. It is obvious that the LO cross section $\hat{\sigma}_{LO}^{kl}$ is IR divergent when we integrate the Feynman amplitude squared $|\mathcal{M}_{LO}^{kl}|^2$ over the full three-body final state phase-space. The divergence arises from the integration over the phase-space region where the final gluon is soft or the final gluon/light-quark jet becomes

collinear to one of the initial partons. To avoid these IR singularities and obtain an IR-safe result, we should take a transverse momentum cut for final jet.

The LO total cross sections for $p\bar{p}(pp) \rightarrow W^-H^0j + X$ can be expressed as

$$\sigma_{LO}(AB(p\bar{p}, pp) \rightarrow W^-H^0j + X) = \sum_{kl=\bar{u}d, \bar{u}s, \bar{u}g, dg}^{\bar{c}d, \bar{c}s, \bar{c}g, sg} \int dx_A dx_B [G_{k/A}(x_A, \mu_f) G_{l/B}(x_B, \mu_f) \hat{\sigma}_{LO}^{kl}(x_A x_B s, \mu_f) + (A \leftrightarrow B)]. \quad (2.6)$$

There μ_f is the factorization energy scale; x_A and x_B describe the fractions of partons k and l in hadrons (proton or antiproton) A and B respectively, with the definitions of

$$x_A = \frac{p_1}{P_A}, \quad x_B = \frac{p_2}{P_B}, \quad (2.7)$$

where P_A and P_B are the four-momenta of the incoming hadrons A and B. $G_{i/H}$ ($i = u, d, c, s, g$, $H = p, \bar{p}$) represent the PDFs of parton i in hadron H . Analogous to Eq.(2.7), we can obtain the expression for $\sigma_{LO}(AB(p\bar{p}, pp) \rightarrow W^+H^0j + X)$. For the LO calculation we use the CTEQ6L1 PDFs[10].

3. NLO QCD corrections

3.1 Virtual corrections

In our numerical calculations we find if we take the nondiagonal Cabibbo-Kobayashi-Maskawa(CKM) matrix, the contributions to the LO cross section for $p\bar{p}(pp) \rightarrow W^\pm H^0j + X$ from the partonic processes involving the coupling between the W^\pm -boson and quarks in two different generations(i.e., $W^+ - \bar{u} - s$ ($W^- - u - \bar{s}$) and/or $W^+ - \bar{c} - d$ ($W^- - c - \bar{d}$) couplings) are less than 1.2% and 5% at the Tevatron and the LHC, respectively. Therefore, it is reasonable to consider only the NLO QCD corrections of partonic processes involving the coupling of the W^\pm -boson with quarks in the same generation in our NLO calculations.

The virtual QCD corrections are evaluated in the 't'Hooft-Feynman gauge. We adopt the dimensional regularization (DR) scheme to regulate the UV and IR divergences and the modified minimal subtraction(\overline{MS}) scheme to renormalize the relevant fields. The one-loop diagrams are essentially obtained from the tree-level diagrams of related partonic processes of W^-H^0j

production, and modify the LO cross sections for partonic processes (2.1)-(2.3). These corrections are induced by self-energy, vertex, box(4-point) and counterterm diagrams. The one-loop level Feynman diagrams and corresponding amplitudes are generated by using the FeynArts3.4 package[11]. The amplitudes which involve UV and IR singularities, are further analytically simplified by the modified FormCalc programs[12]. The final amplitudes are translated into Fortran codes with the UV and IR “ $\epsilon \times$ N-point integral” terms remained unprocessed. The output amplitudes are further numerically evaluated by using our developed Fortran subroutines for calculating N-point integrals and extracting the remaining finite $\epsilon^{\frac{1}{2}}$ terms. In these Fortran codes the IR singularities are separated from the IR-finite remainder by adopting the expressions for the IR singularity in N-point integrals($N \geq 3$) in terms of 3-point integrals[13]. The whole reduction of tensor integrals to the lower-rank tensors and further to the scalar integral is done with the help of the LoopTools library [12, 14], and the FF package [15]. The dimensionally regularized soft or collinear singular 3- and 4-point integrals had to be added to this library. The virtual corrections to the partonic processes $kl \rightarrow W^- H^0 j$ can be expressed as

$$d\hat{\sigma}_V^{kl}(\hat{s}) = \frac{1}{2\hat{s}} \sum 2Re \left(\mathcal{M}_{LO}^{kl\dagger} \mathcal{M}_V^{kl} \right) d\Omega_3^{kl}, \quad (kl = \bar{q}q', \bar{q}g, q'g), \quad (3.1)$$

where we use the same notations as in Eq.(2.4); \mathcal{M}_V^{kl} represents the renormalized one-loop amplitude for the kl annihilation partonic process. In both the LO and NLO calculations for the $W^- H^0 j$ production at the Tevatron and the LHC we should involve all the contributions of the partonic processes $kl \rightarrow W^- H^0 j$ where $kl = \bar{u}d, \bar{u}s, \bar{c}d, \bar{c}s, \bar{u}g, \bar{c}g, dg, sg$.

There exist both ultraviolet(UV) and soft/collinear infrared(IR) singularities in the loop corrections to the partonic process $kl \rightarrow W^- H^0 j$, but the total NLO QCD amplitude of the subprocess is UV finite after performing the renormalization procedure. Nevertheless, it still contains soft/collinear IR singularities. The soft/collinear IR singularities can be cancelled by adding the contributions of the real gluon/light-(anti)quark emission partonic processes, and redefining the parton distribution functions at the NLO.

3.2 Real gluon and light-(anti)quark emission corrections

The real gluon and light-(anti)quark emission partonic processes are obtained from the matrix elements of $0 \rightarrow W^- H^0 gg \bar{q}' q$ and $0 \rightarrow W^- H^0 q \bar{q}' q'' \bar{q}''$ by all possible crossings of (anti)quarks (q , q' and q'') and gluons into the initial state. The relevant real correction partonic processes can be grouped as: (1) $gg \rightarrow W^- H^0 \bar{q}' q$, (2) $\bar{q} q' \rightarrow W^- H^0 gg$, (3) $g \bar{q} \rightarrow W^- H^0 g \bar{q}'$, (4) $g q' \rightarrow W^- H^0 g q$, (5) $\bar{q} q' \rightarrow W^- H^0 q'' \bar{q}''$, (6) $\bar{q} \bar{q}'' \rightarrow W^- H^0 \bar{q}' \bar{q}''$, (7) $q'' \bar{q} \rightarrow W^- H^0 \bar{q}' q''$, (8) $q'' \bar{q}'' \rightarrow W^- H^0 q \bar{q}'$, (9) $q' \bar{q}'' \rightarrow W^- H^0 q \bar{q}''$, (10) $q' q'' \rightarrow W^- H^0 q q''$. There the quark notations represent $q = u, c$, $q' = d, s$ and $q'' = u, d, c, s, b$, respectively. Since the (anti)bottom PDF in the (anti)proton is heavily suppressed with respect to the other light quarks, we neglect the real emission partonic processes which involve the (anti)bottom quark in initial states. The real gluon/light-(anti)quark emission partonic channels (1)-(10) at tree-level give the origins of soft and collinear IR singularities. After the summation of the virtual corrections with all the real parton emission corrections, the numerical result is soft IR-safe, while there still exists remained collinear divergence. But it will be totally IR safe when we include the contributions from the collinear counterterms of the PDFs.

The IR singularities of the real parton emission subprocesses can be isolated by adopting the two cutoff phase-space slicing (TCPSS) method[16]. We take the $\bar{q}(p_1)g(p_2) \rightarrow W^-(p_3)H^0(p_4) \bar{q}'(p_5)g(p_6)$ ($q = u, c$, $q' = d, s$) as an example and show how to deal with the calculation of the real emission process. This partonic process contains eight LO Feynman diagrams which are depicted in Fig.2. We can find from Fig.2 that the tree-level real emission subprocess $\bar{q}g \rightarrow W^- H^0 \bar{q}'g$ involves both the soft and collinear singularities due to the gluon/antiquark(\bar{q} , \bar{q}') splitting in this initial or final state. The IR singularities in the partonic process are isolated by applying the TCPSS method. An arbitrary small soft cutoff δ_s is introduced to separate the $2 \rightarrow 4$ phase-space into two regions, $E_6 \leq \delta_s \sqrt{\hat{s}}/2$ (soft gluon region) and $E_6 > \delta_s \sqrt{\hat{s}}/2$ (hard gluon region). Another cutoff δ_c is used to decompose the hard region into a hard collinear(HC) region and hard noncollinear (\overline{HC}) region to isolate the remaining collinear singularity from the soft IR-safe hard region. The criterion for separating the HC region is described as below: The region for real gluon/light-quark emission with $\hat{s}_{16}(\hat{s}_{25}, \hat{s}_{26}, \hat{s}_{56}) < \delta_c \hat{s}$ (where $\hat{s}_{ij} = (p_i + p_j)^2$)

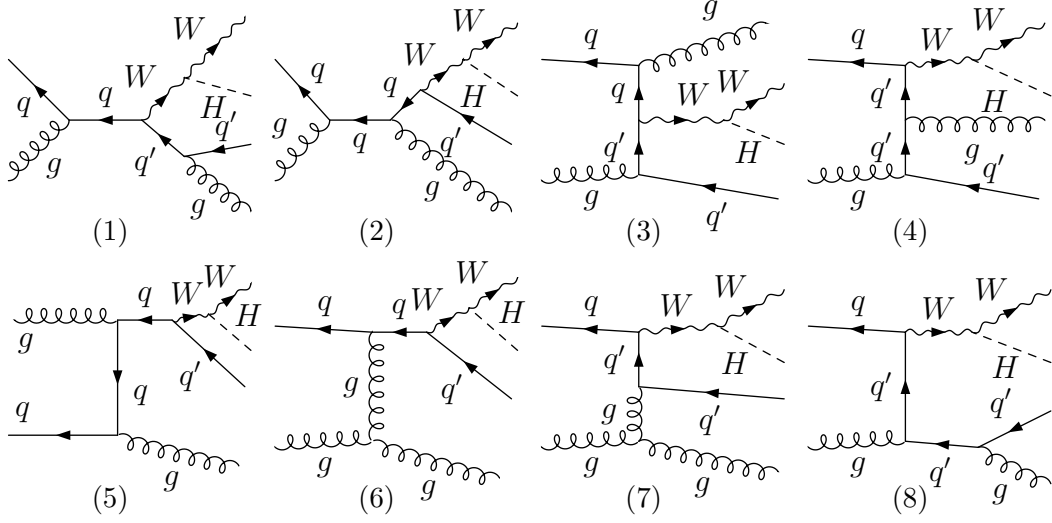


Figure 2: The tree-level Feynman diagrams for the real emission process $\bar{q}g \rightarrow W^- H^0 \bar{q}'g$.

is called the HC region. Otherwise it is called the \overline{HC} region. Then the cross section for the real emission partonic process $\bar{q}g \rightarrow W^- H^0 \bar{q}'g$ can be written as

$$\hat{\sigma}_R(\bar{q}g \rightarrow W^- H^0 \bar{q}'g) = \hat{\sigma}^S + \hat{\sigma}^H = \hat{\sigma}^S + \hat{\sigma}^{HC} + \hat{\sigma}^{\overline{HC}}. \quad (3.2)$$

3.3 NLO corrected cross sections

The full NLO QCD corrected hadronic cross section for the $W^- H^0 j$ production at hadron colliders can be written as:

$$\sigma_{NLO}(p\bar{p}/pp \rightarrow W^- H^0 j + X) = \int dx_A dx_B \left\{ \sum_{ij} [G_{i/A}(x_A, \mu_f) G_{j/B}(x_B, \mu_f) \hat{\sigma}_{NLO}^{ij}(x_A x_B S, \mu_r)] + (A \leftrightarrow B) \right\}, \quad (3.3)$$

where the notations of μ_f , x_A , x_B are the same as those in Eq.(2.6), but we adopt the CTEQ6m PDFs[10] for $G_{i/A}(x_A, x_B, \mu_f)$ and $G_{j/B}(x_A, x_B, \mu_f)$ in the NLO calculations. The total NLO QCD corrected cross section for the partonic process $kl \rightarrow W^- H^0 j$ can be expressed as

$$\hat{\sigma}_{NLO}^{kl} = \hat{\sigma}_{LO}^{kl} + \Delta \hat{\sigma}_{NLO}^{kl} = \hat{\sigma}_{LO}^{kl} + \hat{\sigma}_R^{kl} + \hat{\sigma}_V^{kl}, \quad (3.4)$$

For simplicity, we define the factorization and renormalization scales being equal, i.e., $\mu_f = \mu_r = \mu$. At the Tevatron the incoming colliding particles are proton and antiproton; the cross

sections for both the $p\bar{p} \rightarrow W^- H^0 j + X$ and $p\bar{p} \rightarrow W^+ H^0 j + X$ processes should be the same. In the following we provide only the results for the former process. On the contrary, we give the LHC results for the $pp \rightarrow W^- H^0 j + X$ and $pp \rightarrow W^+ H^0 j + X$ processes separately because of its proton-proton colliding mode.

4. Numerical results and discussion

In our numerical calculations we take one-loop and two-loop running α_s in the LO and NLO calculations, respectively[17]. The QCD parameters are taken as $\Lambda_5^{LO} = 165 \text{ MeV}$, $\Lambda_5^{\overline{MS}} = 226 \text{ MeV}$, $N_f = 5$. We take the renormalization and factorization scales to be a common value as $\mu_r = \mu_f = \mu_0 \equiv \frac{1}{2}(m_W + m_H)$ and $m_H = 120 \text{ GeV}$ by default. The colliding energies in the proton-(anti)proton center-of-mass system are taken as $\sqrt{s} = 14 \text{ TeV}$ for the LHC and $\sqrt{s} = 1.96 \text{ TeV}$ for the Tevatron Run II. We set the values of the CKM matrix elements as

$$V_{CKM} = \begin{pmatrix} V_{ud} & V_{us} & V_{ub} \\ V_{cd} & V_{cs} & V_{cb} \\ V_{td} & V_{ts} & V_{tb} \end{pmatrix} = \begin{pmatrix} 0.97418 & 0.22577 & 0 \\ -0.22577 & 0.97418 & 0 \\ 0 & 0 & 1 \end{pmatrix}. \quad (4.1)$$

The cosine of the weak mixing angle squared is set to its on-shell value obtained by $c_W^2 = m_W^2/m_Z^2$. The weak vector boson and top-quark masses are taken as $m_W = 80.398 \text{ GeV}$, $m_Z = 91.1876 \text{ GeV}$ and $m_t = 171.2 \text{ GeV}$. The fine structure constant at the Z^0 -pole has the value as $\alpha(m_Z^2)^{-1} = 127.925$ [17].

In the LO and NLO calculations we adopt the massless five-flavor scheme and put the restriction of $p_T^j > p_{T,j}^{cut}$ on the jet transverse momentum for one-jet events. For the two-jet events (originating from the real corrections), we apply the jet algorithm of Ref.[18] in the definition of the tagged hard jet with $R = 1$. That means when two jets in the final state satisfy the constraint of $\sqrt{\Delta\eta^2 + \Delta\phi^2} < R \equiv 1$ (where $\Delta\eta$ and $\Delta\phi$ are the differences of rapidity and azimuthal angle between the two jets), we merge them into one new “jet” and consider it as an one-jet event. In handling the one- and two-jet events we use the so called “inclusive” scheme in default of other statement. In this scheme we demand $p_T^j > p_{T,j}^{cut}$ for the one-jet events, and for the two-jet events we apply the constraint of $p_T^j > p_{T,j}^{cut}$ on the leading jet but not on the second jet, where the leading jet and the second jet are characterized by

$E_T(\text{the leading jet}) > E_T(\text{the second jet})$.

Since the events involving the final hard $b(\bar{b})$ -jet can be experimentally excluded by anti b -tagging, we consider only the phase-space with $b\bar{b}$ jets satisfying $\sqrt{\Delta\eta^2 + \Delta\phi^2} < 1$ for each partonic $W^\pm H^0 b\bar{b}$ production process. For these events, the final b and \bar{b} are accepted as one hard “jet” when its transverse momentum $p_T^j > p_{T,j}^{cut}$.

In order to verify the correctness of our results, we made following verifications:

1. The UV and IR safeties are verified numerically after combining all the contributions at the NLO.
2. The LO cross section for the process $p\bar{p} \rightarrow \bar{u}d \rightarrow W^- H^0 j + X$ at the Tevatron was calculated by using two independent developed programs: FeynArts3.4/FormCalc5.4 [11, 12] and CompHEP-4.4p3 programs[19], and applying the Feynman and unitary gauges separately. The results are in agreement within the statistic errors. The virtual correction and the real gluon/light-(anti)quark correction to the $pp \rightarrow W^- H^0 j + X$ process at the LHC were evaluated twice independently based on different codes, and yield results in mutual agreement.
3. The total NLO QCD correction being independent of the two cutoffs, δ_s and δ_c , has been numerically verified. In Figs.3(a) and (b) we depict the total NLO QCD corrections to the $p\bar{p} \rightarrow W^- H^0 j + X$ process at the Tevatron as the functions of the cutoffs δ_s and δ_c . There we apply the inclusive scheme with $p_{T,j}^{cut} = 20 \text{ GeV}$, and take $\mu = \mu_0$, $m_H = 120 \text{ GeV}$, $\delta_c = \delta_s/50$. The amplified curve for $\Delta\sigma_{NLO}$ of Fig.3(a) is presented in Fig.3(b) together with calculation errors. The figures demonstrate that the total NLO QCD correction does not depend on the arbitrarily chosen value of the cutoff $\delta_s(\delta_c)$ within statistic errors. Figure 3(a) shows that although the three-body correction($\Delta\sigma^{(3)}$) and four-body correction($\Delta\sigma^{(4)}$) are strongly related with the cutoff $\delta_s(\delta_c)$, the final total NLO QCD correction $\Delta\sigma_{NLO}$ which is the summation of the three-body term and four-body term, i.e., $\Delta\sigma_{NLO} = \Delta\sigma^{(3)} + \Delta\sigma^{(4)}$, is independent of the two cutoffs within the statistic errors. The independence of the full NLO QCD corrections to the $p\bar{p} \rightarrow W^- H^0 j + X$

process on the cutoffs δ_s and δ_c provides an indirect check for the correctness of the calculations. In further numerical calculations, we fix $\delta_s = 5 \times 10^{-4}$ and $\delta_c = \delta_s/50$.

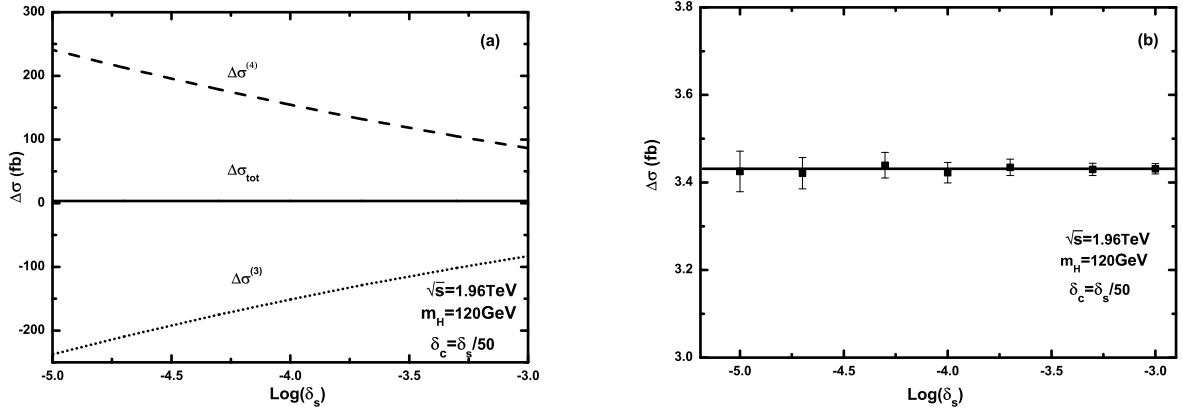


Figure 3: (a) the dependence of the NLO QCD corrections to the $p\bar{p} \rightarrow W^- H^0 j + X$ process on the soft cutoff δ_s and δ_c at the Tevatron, where we take $\delta_c = \delta_s/50$, $\mu = \mu_0$, $m_H = 120 \text{ GeV}$, and apply the inclusive scheme with $p_{T,j}^{cut} = 20 \text{ GeV}$. (b) the amplified curve for $\Delta\sigma_{NLO}$ of Fig.3(a).

In Figs.4(a), (b) and (c) we present the scale dependence of the LO, NLO cross sections, and the corresponding K-factor($K(\mu) \equiv \sigma_{NLO}(\mu)/\sigma_{LO}(\mu)$) upon varying renormalization and factorization scales in the $\mu \equiv \mu_r = \mu_f$ way for the $p\bar{p} \rightarrow W^- H^0 j + X$ process at the Tevatron and the $pp \rightarrow W^\mp H^0 j + X$ processes at the LHC, separately. There we adopt the inclusive scheme with $p_{T,j}^{cut} = 20 \text{ GeV}$. Figure 4(a) shows that when the curve transits from LO to the NLO, the scale uncertainty (defined in the range of $0.5\mu_0 < \mu < 2\mu_0$) is reduced by the NLO QCD corrections from 44.6%(LO) to 11.9%(NLO) at the Tevatron. Figures 4(b,c) show that the scale uncertainties(defined in the range of $0.5\mu_0 < \mu < 2\mu_0$) at the LHC are reduced from 20.1%(LO) to 4.2%(NLO) for the $pp \rightarrow W^- H^0 j + X$ process and from 20.0%(LO) to 4.7%(NLO) for the $pp \rightarrow W^+ H^0 j + X$ process, respectively. We can read from these figures that the K-factor($K(\mu) \equiv \sigma_{NLO}(\mu)/\sigma_{LO}(\mu)$) for the process $p\bar{p} \rightarrow W^- H^0 j + X$ at the Tevatron is in the range of $[0.31, 1.31]$, while the K-factors for the processes $pp \rightarrow W^- H^0 j + X$ and $pp \rightarrow W^+ H^0 j + X$ at the LHC, vary in the ranges of $[0.89, 1.23]$ and $[0.86, 1.19]$ in the plotted

μ/μ_0 ranges, respectively.

In our NLO calculation, we find that the LO, NLO QCD corrected cross sections and the QCD K-factors for the $pp \rightarrow W^- H^0 j + X$ and $pp \rightarrow W^+ H^0 j + X$ processes at the LHC are sensitive to both the transverse momentum cut on the leading jet, $p_{T,j}^{cut}$, and the jet event selection scheme. In order to demonstrate this influence, we present the LO, NLO QCD corrected cross sections and the QCD K-factors for $pp \rightarrow W^- H^0 j + X$ and $pp \rightarrow W^+ H^0 j + X$ processes at the LHC with $p_{T,j}^{cut} = 50 \text{ GeV}$ in Figs.5(a) and (b), respectively. The curves labeled with “NLO(I)” and “NLO(II)” correspond to the NLO QCD corrected cross sections with two different jet event selection schemes: (i) the “inclusive” scheme as declared above; (ii) the “exclusive” scheme, which means the one-jet events with $p_T^j > p_{T,j}^{cut}$ are accepted, and the two-jet events with p_T^j (the second hard jet) $> p_{T,j}^{cut}$ are vetoed[20]. We can see from Figs.5(a) and (b) that the NLO QCD corrections can significantly reduce the factorization/renormalization scale dependence. By adopting the inclusive selection scheme, the LHC LO scale uncertainty (defined in the range of $0.5\mu_0 < \mu < 2\mu_0$) for the $pp \rightarrow W^- H^0 j + X$ process (the $pp \rightarrow W^+ H^0 j + X$ process) is about 23.5%(23.3%), and is reduced to about 10.1%(9.91%) by the NLO QCD corrections. Alternatively when a veto against the emission of a second hard jet is applied (i.e., by adopting the exclusive scheme), the LHC scale uncertainty (defined in the range $0.5\mu_0 < \mu < 2\mu_0$) of the $pp \rightarrow W^- H^0 j + X$ process (the $pp \rightarrow W^+ H^0 j + X$ process) is improved by the NLO QCD correction to the value of 2.06%(3.53%). It shows that the reduction of the scale uncertainty by the exclusive LHC NLO correction is larger than the inclusive NLO correction. From Figs.5(a,b) we can see that by taking $p_{T,j}^{cut} = 50 \text{ GeV}$, the exclusive LHC NLO cross section for the $pp \rightarrow W^- H^0 j + X$ process (or the $pp \rightarrow W^+ H^0 j + X$ process) decreases in the low scale region as shown by the curves labeled with “NLO(II)”. Therefore, we can conclude that the curve feature of the LHC NLO QCD corrected cross section for the $pp \rightarrow W^- H^0 j + X$ or the $pp \rightarrow W^+ H^0 j + X$ process versus scale μ is correlated to the $p_{T,j}^{cut}$ value and the jet event selection scheme.

In Table 1 we list some of the representative numerical results for the LO, NLO corrected cross sections and their corresponding K-factors by applying the inclusive scheme with $p_{T,j}^{cut} =$

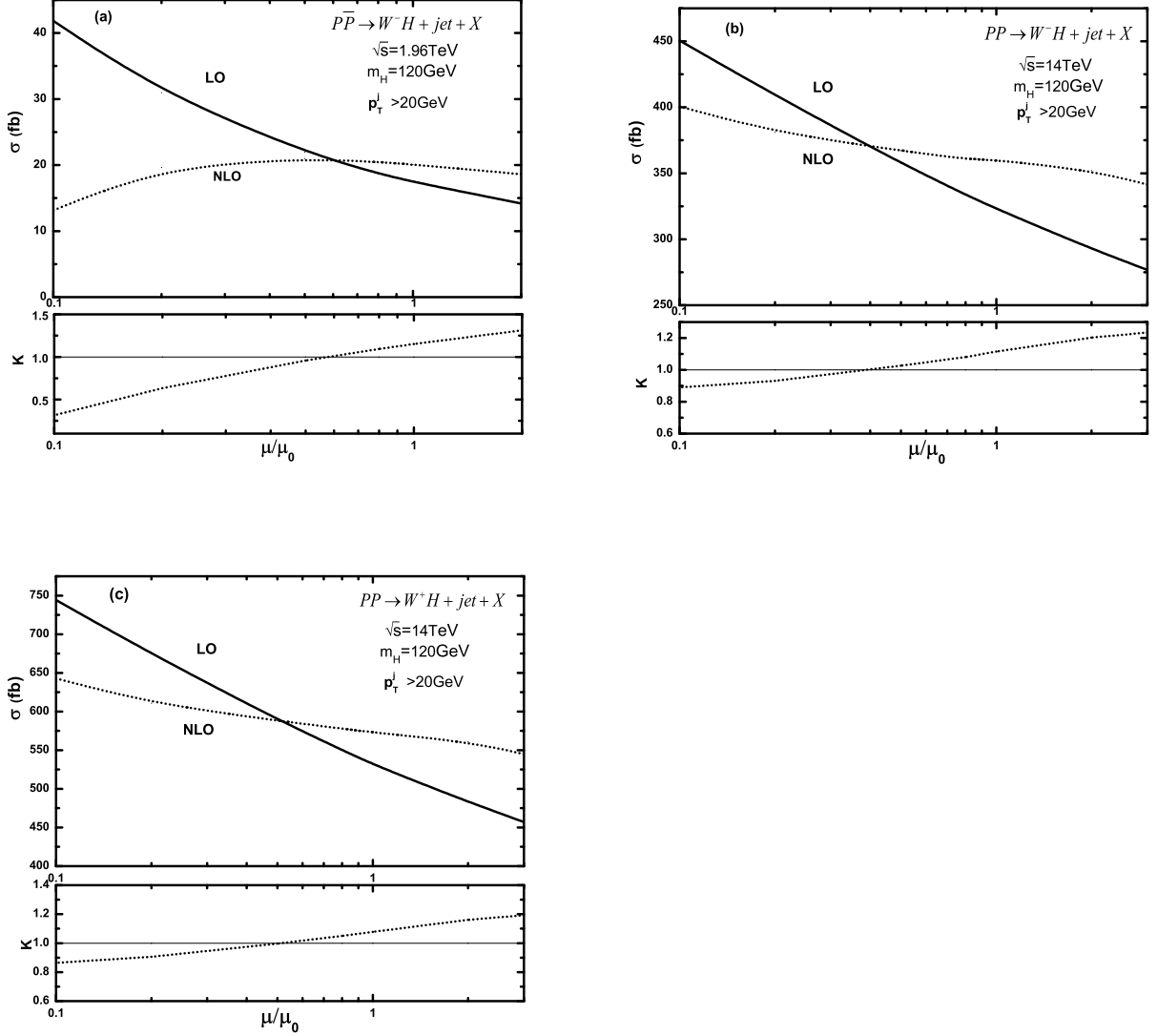


Figure 4: The LO, NLO corrected cross sections and the corresponding K-factor ($K(\mu) \equiv \sigma_{NLO}(\mu)/\sigma_{LO}(\mu)$) versus the factorization/renormalization scale ($\mu = \mu_r = \mu_f$) by applying the inclusive scheme with $p_{T,j}^{cut} = 20 \text{ GeV}$. (a) for $p\bar{p}/pp \rightarrow W^- H^0 j + X$ at the Tevatron, (b) for $pp \rightarrow W^- H^0 j + X$ at the LHC, (c) For $pp \rightarrow W^+ H^0 j + X$ at the LHC.

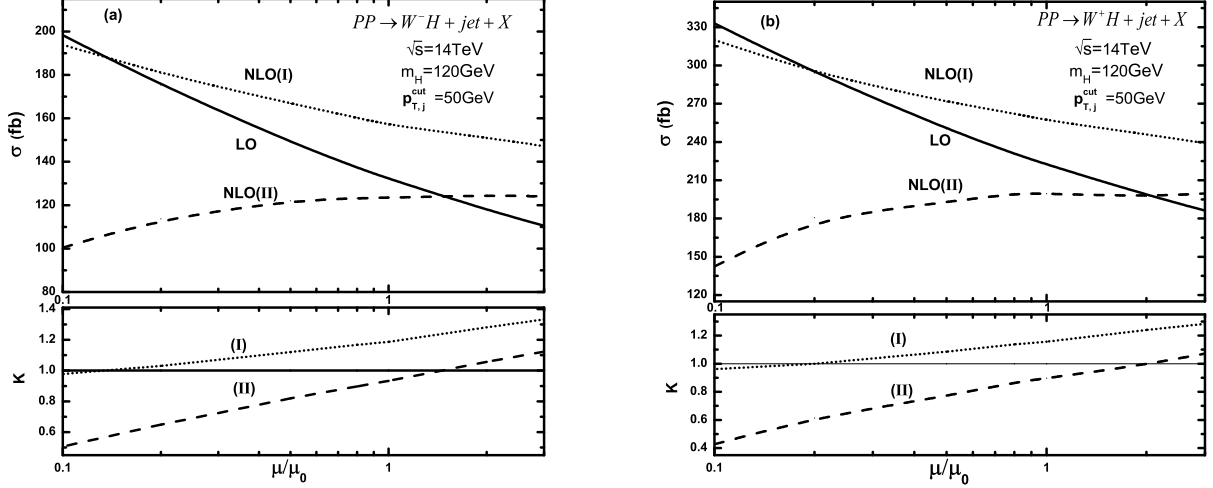


Figure 5: The LO, NLO corrected cross sections and the corresponding K-factor($K(\mu) \equiv \sigma_{NLO}(\mu)/\sigma_{LO}(\mu)$) at the LHC by taking $p_{T,j}^{cut} = 50 \text{ GeV}$ and adopting separately (I) the inclusive scheme and (II) exclusive scheme. (a) for $pp \rightarrow W^- H^0 j + X$, (b) for $pp \rightarrow W^+ H^0 j + X$.

20 GeV, and taking $m_H = 120 \text{ GeV}$, the energy scale $\mu = 0.5\mu_0, \mu_0, 2\mu_0, \mu_1$ and μ_2 separately, where μ_1 and μ_2 are phase-space dependent scales defined as $\mu_1 \equiv \sqrt{\frac{1}{2} \left((p_T^W)^2 + (p_T^H)^2 + m_W^2 + m_H^2 \right)}$ and $\mu_2 \equiv \sqrt{(p_T^W)^2 + (p_T^H)^2 + m_W^2 + m_H^2}$.

In Table 2, we list some of the numerical results of the LO and the QCD corrected cross sections and the corresponding K-factors($K \equiv \frac{\sigma_{NLO}}{\sigma_{LO}}$) for the $p\bar{p} \rightarrow W^- H^0 j + X$ process at the Tevatron and the $pp \rightarrow W^\pm H^0 j + X$ processes at the LHC, where we apply the inclusive scheme with $p_{T,j}^{cut} = 20 \text{ GeV}$, and take $\mu = \mu_0$, the values of Higgs-boson mass as 120 GeV, 150 GeV and 180 GeV, separately. Table 2 shows both the LO and NLO QCD corrected cross sections and K-factors are all sensitive to the Higgs mass. Among them the K-factor for the $pp \rightarrow W^+ H^0 j + X$ process at the LHC is less sensitive to the Higgs boson mass than others. We also find the LO and the NLO QCD corrected cross sections decrease rapidly with the increment of m_H at both hadronic colliders.

In Figs.6(a,b,c) we depict the LO and NLO QCD corrected differential cross sections of the transverse momenta for the final produced H^0 -, W^- -boson and leading jet in the process $p\bar{p} \rightarrow W^- H^0 j + X$ at the Tevatron, and the corresponding K-factors($K(p_T) \equiv \frac{d\sigma_{NLO}}{dp_T} / \frac{d\sigma_{LO}}{dp_T}$),

Process	$\mu(GeV)$	$\sigma_{LO}(fb)$	$\sigma_{NLO}(fb)$	K
$p\bar{p} \rightarrow W^- H^0 j + X$ $\sqrt{s} = 1.96 TeV$	$0.5\mu_0$	21.949(3)	21.01(2)	0.96
	μ_0	17.440(2)	20.08(2)	1.15
	$2\mu_0$	14.167(2)	18.61(1)	1.31
	μ_1	16.0128(8)	19.60(1)	1.22
	μ_2	14.457(1)	18.79(1)	1.30
$pp \rightarrow W^- H^0 j + X$ $\sqrt{s} = 14 TeV$	$0.5\mu_0$	357.58(2)	367.2(2)	1.03
	μ_0	323.03(2)	360.2(2)	1.12
	$2\mu_0$	292.76(2)	352.1(2)	1.20
	μ_1	306.023(8)	350.9(1)	1.15
	μ_2	291.63(1)	347.9(1)	1.19
$pp \rightarrow W^+ H^0 j + X$ $\sqrt{s} = 14 TeV$	$0.5\mu_0$	589.49(5)	588.0(3)	0.997
	μ_0	531.37(3)	572.9(3)	1.08
	$2\mu_0$	483.21(4)	561.0(3)	1.16
	μ_1	503.36(2)	561.2(2)	1.12
	μ_2	479.93(2)	556.4(2)	1.16

Table 1: The numerical results for the LO, NLO QCD corrected cross sections and their corresponding K-factors($K(\mu) \equiv \sigma_{NLO}(\mu)/\sigma_{LO}(\mu)$) by applying the inclusive scheme with $p_{T,j}^{cut} = 20 GeV$, and taking $m_H = 120 GeV$ and different values of scale μ for the process $p\bar{p} \rightarrow W^- H^0 j + X$ at the Tevatron Run II, the processes $pp \rightarrow W^- H^0 j + X$ and $pp \rightarrow W^+ H^0 j + X$ at the LHC. In this table we denote $\mu_0 = \frac{1}{2}(m_W + m_H)$, $\mu_1 = \sqrt{\frac{1}{2} \left[(p_T^W)^2 + (p_T^H)^2 + m_W^2 + m_H^2 \right]}$ and $\mu_2 = \sqrt{(p_T^W)^2 + (p_T^H)^2 + m_W^2 + m_H^2}$.

process	$m_H(GeV)$	$\sigma_{LO}(fb)$	$\sigma_{NLO}(fb)$	K
$p\bar{p} \rightarrow W^- H^0 j + X$	120	17.440(2)	20.08(2)	1.15
	150	8.2697(8)	9.306(7)	1.13
	$\sqrt{s} = 1.96TeV$	180	4.2729(4)	4.629(3)
$pp \rightarrow W^- H^0 j + X$	120	323.03(2)	360.2(2)	1.12
	150	164.96(1)	180.94(8)	1.10
	$\sqrt{s} = 14TeV$	180	93.692(6)	100.26(4)
$pp \rightarrow W^+ H^0 j + X$	120	531.37(3)	572.9(3)	1.08
	150	284.49(2)	294.2(2)	1.03
	$\sqrt{s} = 14TeV$	180	166.18(1)	167.9(1)

Table 2: The numerical results for the LO and the NLO QCD corrected cross sections and the corresponding K-factor ($K \equiv \frac{\sigma_{NLO}}{\sigma_{LO}}$) with $\mu = \mu_0$, $m_H = 120 GeV$, $150 GeV$ and $180 GeV$, for the $p\bar{p} \rightarrow W^- H^0 j + X$ process at the Tevatron and the $pp \rightarrow W^\pm H^0 j + X$ processes at the LHC by applying the inclusive scheme with $p_{T,j}^{cut} = 20 GeV$.

separately. There we adopt the inclusive scheme with $p_{T,j}^{cut} = 20 GeV$ and take $m_H = 120 GeV$. The distributions in these figures marked with (I) and (II) are for the $\mu = \mu_1$ and $\mu = \mu_0$ respectively. The analogous plots for the processes $pp \rightarrow W^- H^0 j + X$ and $pp \rightarrow W^+ H^0 j + X$ at the LHC are depicted in Figs.7(a,b,c) and Figs.8(a,b,c), respectively. In these figures we provide the NLO QCD corrected differential cross sections ($\frac{d\sigma_{NLO}}{dp_T}$) by applying the inclusive scheme with $p_{T,j}^{cut} = 20 GeV$. The plot for $\frac{d\sigma_{NLO}}{dp_T^j}$ refers to the distribution of the transverse momentum of the leading jet. Figures.6(a,b), Figs.7(a,b) and Figs.8(a,b) show that at both the Tevatron and the LHC the NLO QCD corrections significantly enhance the LO differential cross sections of p_T^H and p_T^W , especially when $p_T^H, p_T^W < 150 GeV$. We observe also that the curves for the $K(p_T^H)$ - and $K(p_T^W)$ -factors in these figures become more stable in the transition from $\mu = \mu_0$ to the phase-space dependent scale $\mu = \mu_1$ (i.e., $\mu_1 = \sqrt{\frac{1}{2} [(p_T^W)^2 + (p_T^H)^2 + m_W^2 + m_H^2]}$). We can see from Fig.6(c), Fig.7(c) and Fig.8(c) that most of the leading jets are produced in the low transverse momentum range, and the differential cross section of p_T^j is significantly enhanced by the NLO QCD corrections.

We take the orientation of the incoming antiproton as the z-axis direction at the Tevatron and the orientation of one of the incoming protons as the direction of z-axis at the LHC. The

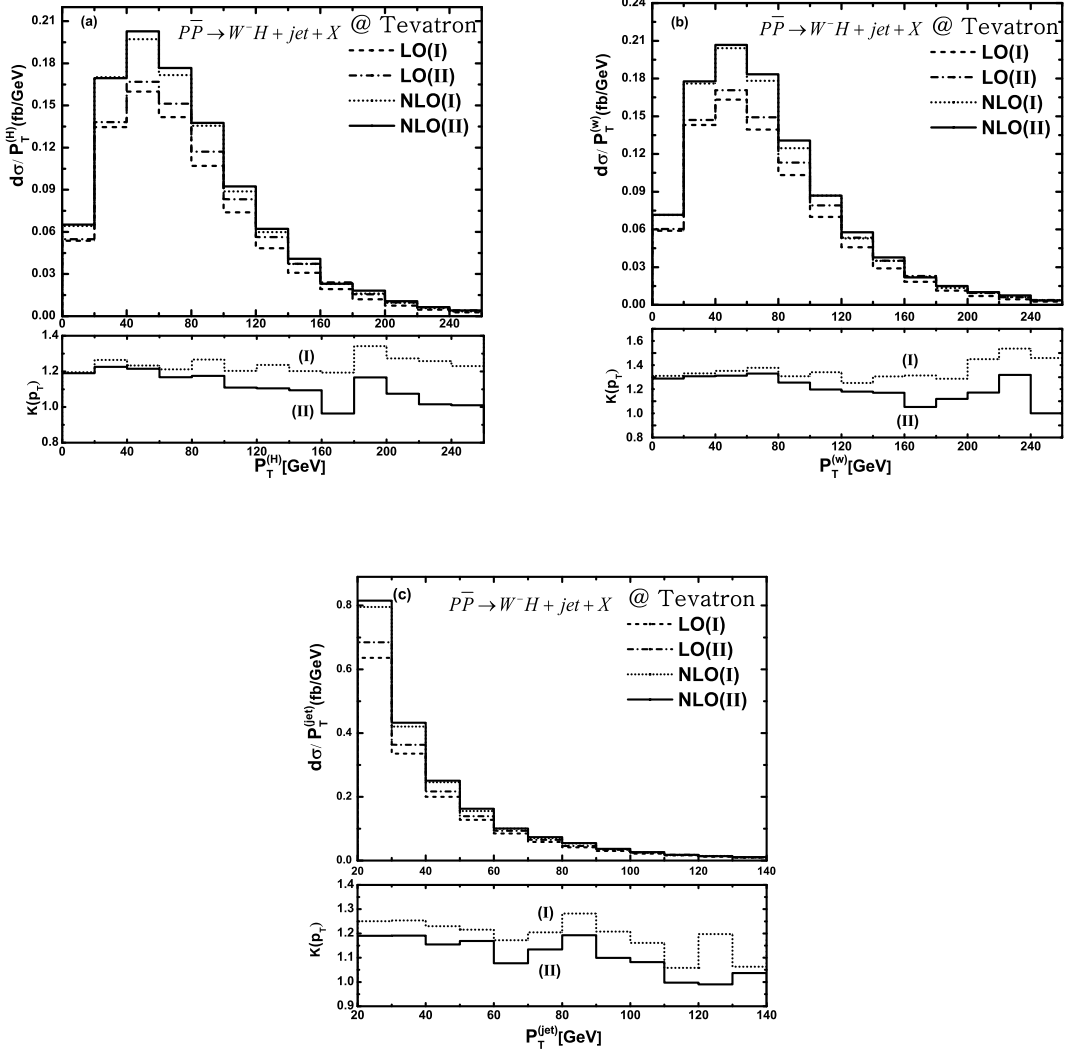


Figure 6: The LO and NLO QCD corrected distributions of the transverse momenta of final particles and corresponding K-factors ($K(p_T) \equiv \frac{d\sigma_{NLO}}{dp_T} / \frac{d\sigma_{LO}}{dp_T}$) for the process $p\bar{p} \rightarrow W^- H^0 j + X$ at the Tevatron with $m_H = 120$ GeV. The distributions labeled by (I) and (II) are for the $\mu = \mu_1$ and $\mu = \mu_0$ respectively. (a) for H^0 -boson, (b) for W^- -boson, (c) for final leading jet.

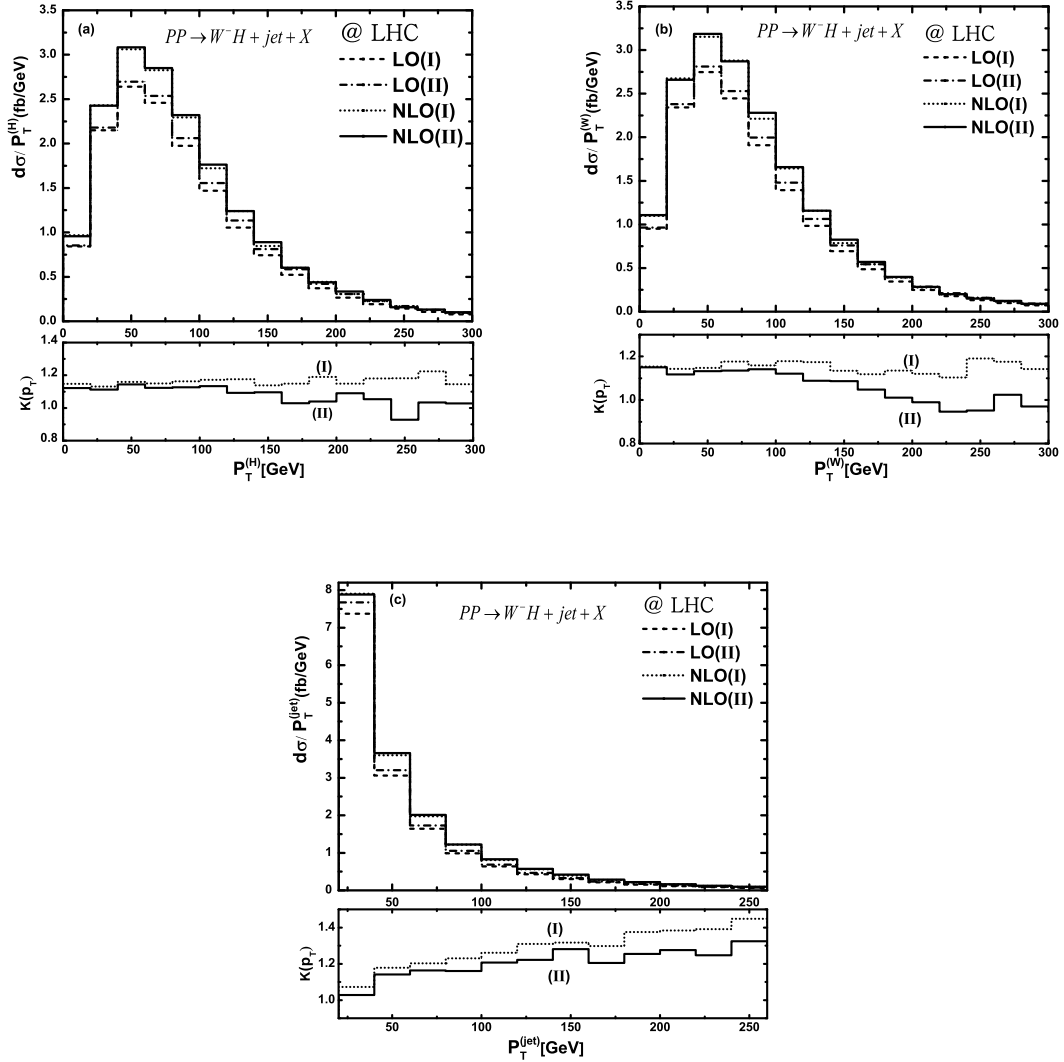


Figure 7: The LO and NLO QCD corrected distributions of the transverse momenta of final particles and corresponding K-factors ($K(p_T) \equiv \frac{d\sigma_{NLO}}{dp_T} / \frac{d\sigma_{LO}}{dp_T}$) for the process $pp \rightarrow W^- H^0 j + X$ at the LHC with $m_H = 120 \text{ GeV}$. The distributions labeled by (I) and (II) are for the $\mu = \mu_1$ and $\mu = \mu_0$ respectively. (a) for H^0 -boson, (b) for W^- -boson, (c) for final leading jet.

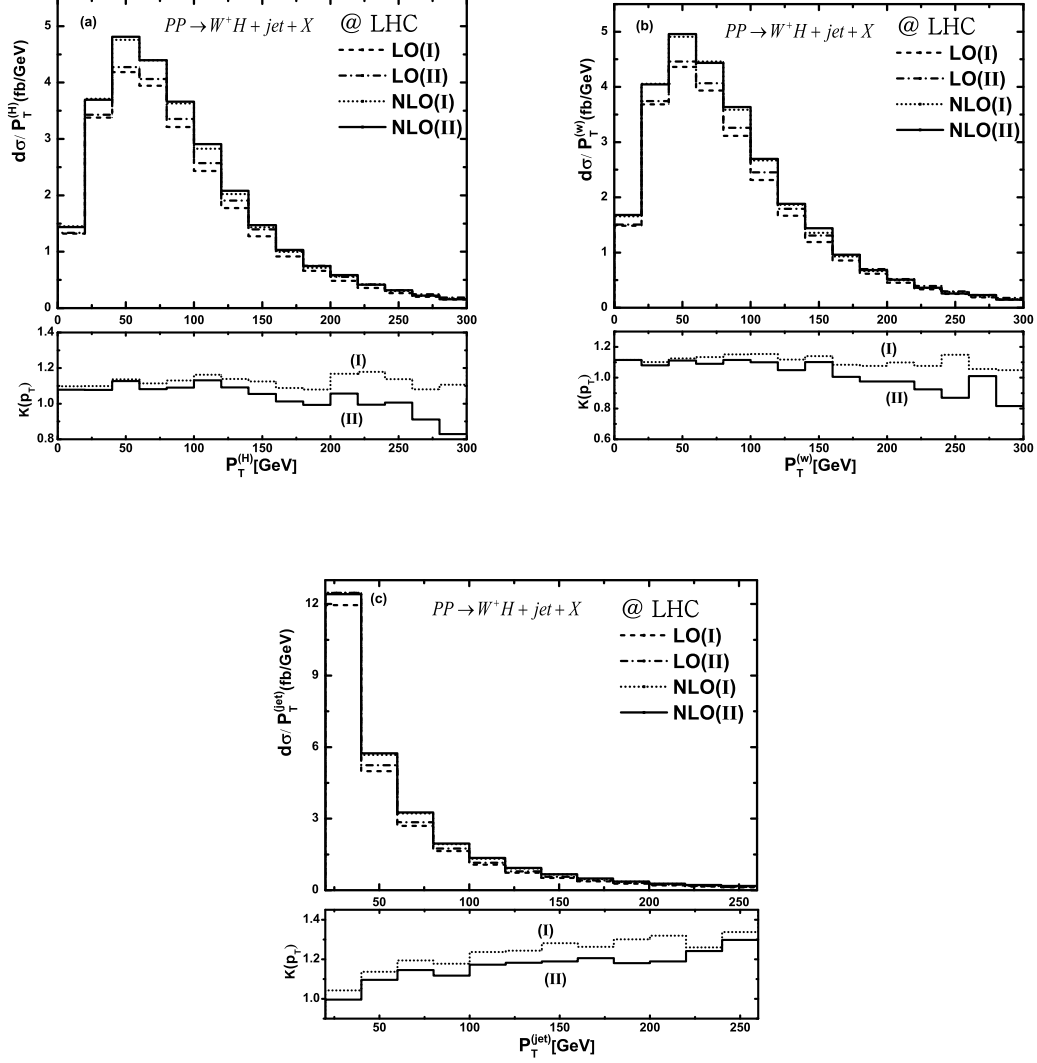


Figure 8: The LO and NLO QCD corrected distributions of the transverse momenta of final particles and corresponding K-factors ($K(p_T) \equiv \frac{d\sigma_{NLO}}{dp_T} / \frac{d\sigma_{LO}}{dp_T}$) for the process $pp \rightarrow W^+ H^0 j + X$ at the LHC with $m_H = 120 \text{ GeV}$. The distributions labeled by (I) and (II) are for the $\mu = \mu_1$ and $\mu = \mu_0$ respectively. (a) for H^0 -boson, (b) for W^+ -boson, (c) for final leading jet.

θ^H (θ^W or θ^j) is define as the H -boson (W -boson or the leading jet) production angle with respect to the z-axis direction for the $W^\pm H^0 j$ production process at the Tevatron or the LHC. In Figs.9(a,b,c), we present the LO and NLO QCD corrected distributions as the functions of the cosines of the H^0 -boson, W^- -boson and leading jet production angles($\frac{d\sigma}{d\cos\theta}$), and their corresponding K-factors($K(\cos\theta) \equiv \frac{d\sigma_{NLO}}{d\cos\theta} / \frac{d\sigma_{LO}}{d\cos\theta}$) at the Tevatron. The NLO distributions in Figs.9(a,b,c) are obtained by applying the inclusive scheme with $p_{T,j}^{cut} = 20 \text{ GeV}$, and taking $m_H = 120 \text{ GeV}$, $\mu = \mu_0$. They show that the produced H^0 -boson, W^- -boson and leading jet slightly prefer to go out in the forward hemisphere region at the Tevatron. In Figs.10(a,b,c) and Figs.11(a,b,c), we present the LO and NLO QCD corrected differential cross sections and their corresponding K-factors as the functions of the cosines of the H^0 -boson, W^- (or W^+)-boson and leading jet production angles for the process $pp \rightarrow W^\pm H^0 j + X$ at the LHC, separately. Again in these figures we apply the inclusive scheme with $p_{T,j}^{cut} = 20 \text{ GeV}$, denote p_T^j as the transverse momentum of the leading jet and set $m_H = 120 \text{ GeV}$, $\mu = \mu_0$. Both the LO and NLO curves in Figs.10(a,b,c) and Figs.11(a,b,c) demonstrate that the outgoing H^0 -boson W^- -boson and leading jet are symmetrically distributed in the forward and backward hemisphere regions.

5. Summary

In this paper we calculate the full NLO QCD corrections to the $W^\pm H^0$ production associated with a jet at the Tevatron Run II and the LHC. We investigate the dependence of the integrated cross sections on the energy scale, and study the NLO QCD contributions to the differential cross sections of the transverse momenta($\frac{d\sigma}{dp_T}$) and the production angle distributions($\frac{d\sigma}{d\cos\theta}$) for the final particles at both hadronic colliders. We find that the NLO QCD radiative corrections obviously modify the LO integrated and differential cross sections, and the NLO QCD corrections to the $W^\pm H^0$ +jet production processes significantly reduce the scale uncertainties of the LO cross sections at both hadron colliders. Our numerical results show that in conditions of applying the inclusive scheme with $p_{T,j}^{cut} = 20 \text{ GeV}$, taking $\mu = \mu_0$ and $m_H = 120 \text{ GeV}$, the K-factor for the process $p\bar{p} \rightarrow W^\pm H^0 j + X$ at the Tevatron Run II is 1.15, while the K-factors for the $pp \rightarrow W^- H^0 j + X$ and $pp \rightarrow W^+ H^0 j + X$ processes at the LHC are 1.12 and 1.08,

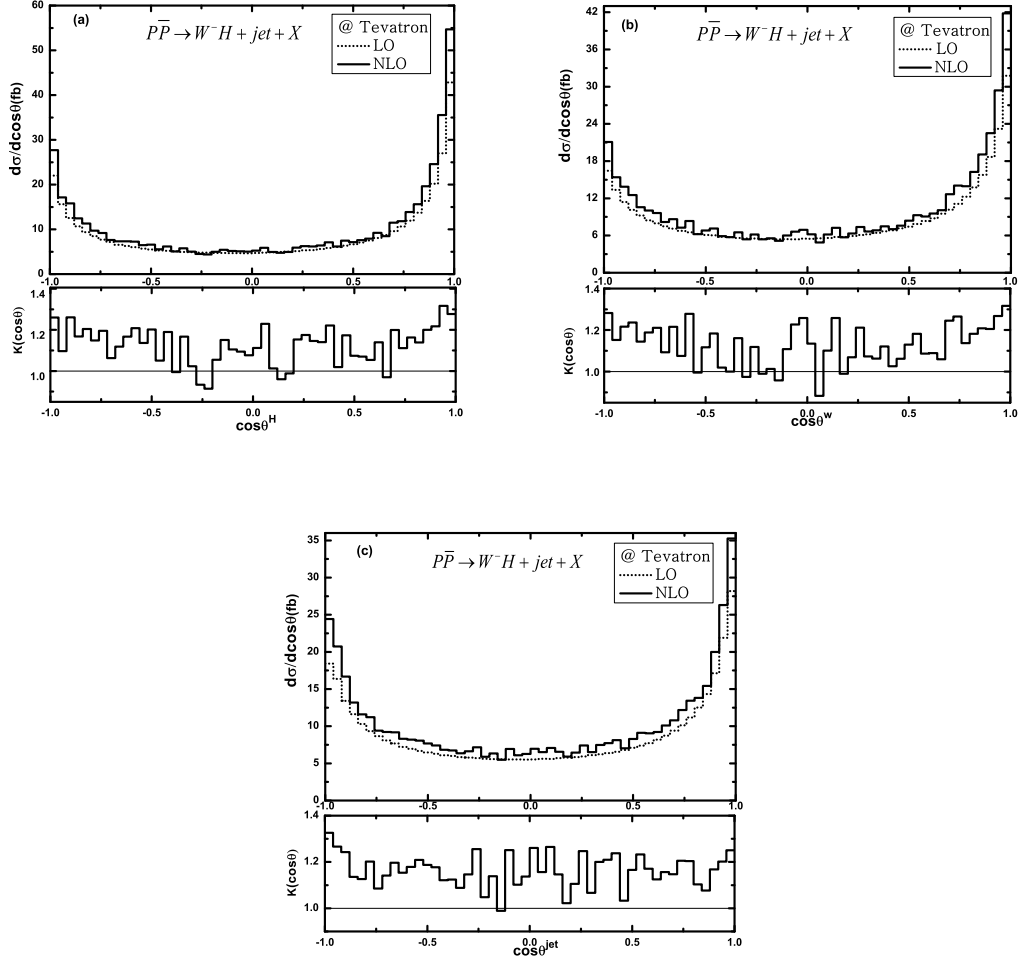


Figure 9: The LO, NLO QCD corrected distributions($\frac{d\sigma}{d\cos\theta}$) and their corresponding K-factors($K(\cos\theta) \equiv \frac{d\sigma_{NLO}}{d\cos\theta} / \frac{d\sigma_{LO}}{d\cos\theta}$) versus the cosine of the angle between the final particle and the direction of the incoming antiproton for the process $p\bar{p} \rightarrow W^- H^0 j + X$ at the Tevatron by applying the inclusive scheme with $p_{T,j}^{cut} = 20 \text{ GeV}$ and taking $\mu = \mu_0$ and $m_H = 120 \text{ GeV}$. (a) for final Higgs-boson, (b) for final W -boson, (c) For final leading jet.

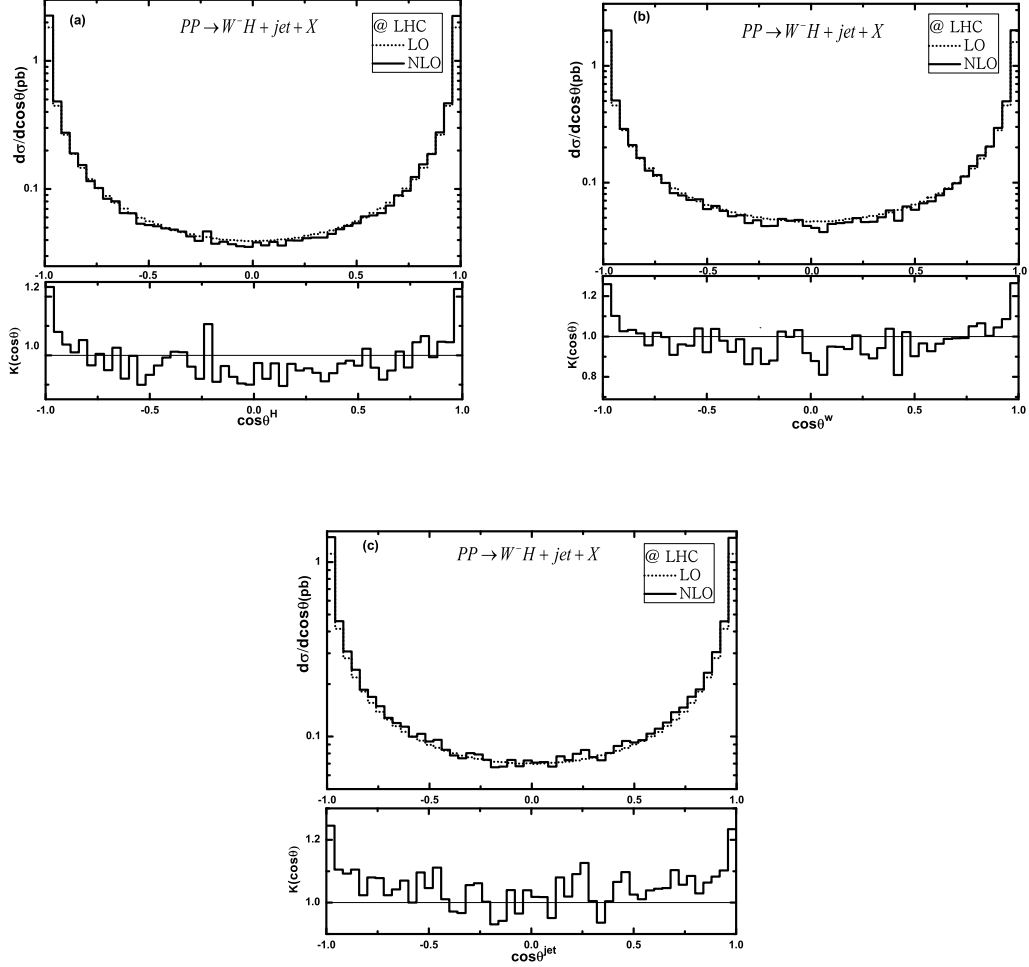


Figure 10: The LO, NLO QCD corrected distributions ($\frac{d\sigma}{d\cos\theta}$) and the corresponding K-factors ($K(\cos\theta) \equiv \frac{d\sigma_{NLO}}{d\cos\theta} / \frac{d\sigma_{LO}}{d\cos\theta}$) versus the cosine of the angle between the final particle and the direction of one of the incoming protons for the process $pp \rightarrow W^- H^0 j + X$ at the LHC by applying the inclusive scheme with $p_{T,j}^{cut} = 20 \text{ GeV}$ and taking $m_H = 120 \text{ GeV}$ and $\mu = \mu_0$. (a) for final Higgs boson, (b) for final W^- -boson, (c) for final leading jet.

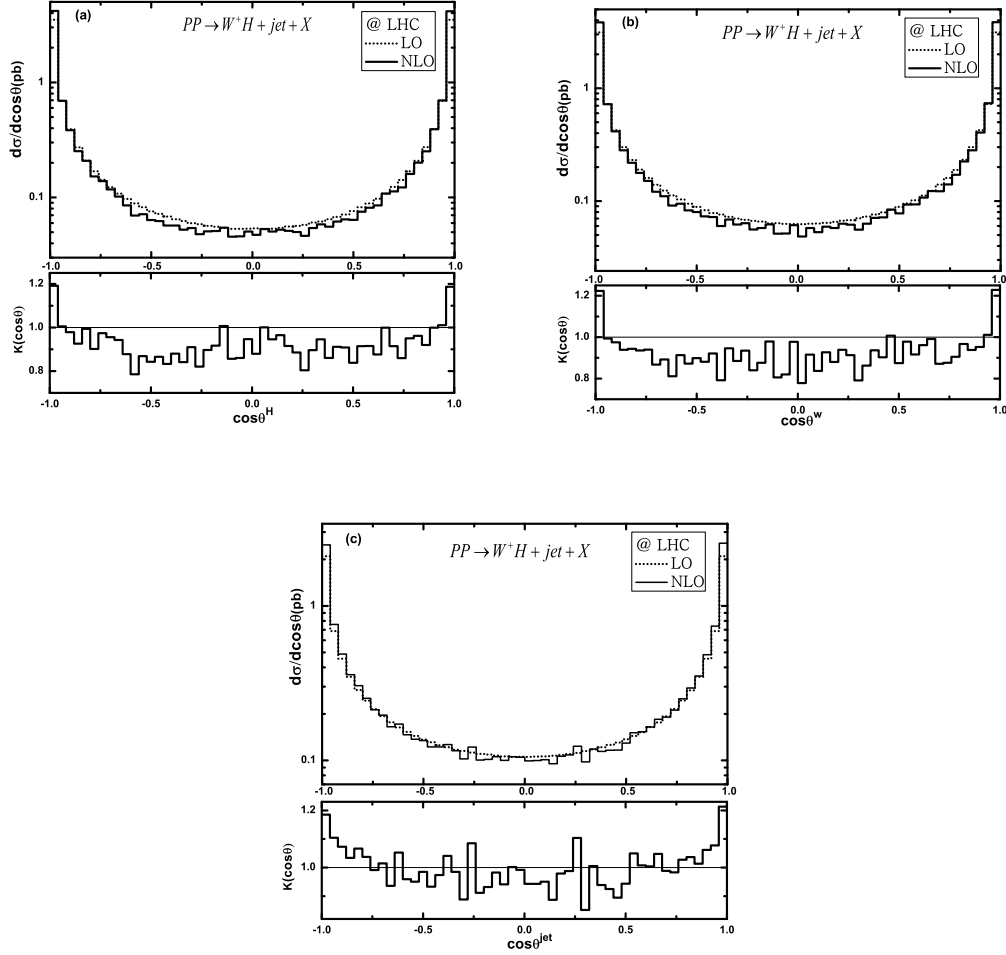


Figure 11: The LO, NLO QCD corrected distributions($\frac{d\sigma}{d\cos\theta}$) and their corresponding K-factor($K(\cos\theta) \equiv \frac{d\sigma_{NLO}}{d\cos\theta} / \frac{d\sigma_{LO}}{d\cos\theta}$) versus the cosine of the angle of the final particle with respect to the direction of one of the incoming protons for the process $pp \rightarrow W^+ H^0 j + X$ at the LHC by applying the inclusive scheme with $p_{T,j}^{cut} = 20 \text{ GeV}$ and taking $m_H = 120 \text{ GeV}$ and $\mu = \mu_0$. (a) for final Higgs boson, (b) for final W^+ -boson, (c) for final leading jet.

respectively. We conclude that in studying the hadronic WH^0 production channel the NLO QCD corrections to the WH^0j production process which is part of inclusive WH^0 production, should be taken into account.

Acknowledgments: This work was supported in part by the National Natural Science Foundation of China(No.10875112), the Specialized Research Fund for the Doctoral Program of Higher Education(SRFDP)(No.20093402110030), the National Science Foundation for Post-doctoral Scientists of China (No.20080440103), and the Funds for Creative Research Program of USTC.

References

- [1] S. L. Glashow, Nucl. Phys. **22** (1961) 579; S. Weinberg, Phys. Rev. Lett. **19** (1967) 1264; A. Salam, Proc. 8th Nobel Symposium Stockholm 1968,ed. N. Svartholm (Almqvist and Wiksells, Stockholm 1968) p.367; H. D. Politzer, Phys. Rep. **14** (1974) 129.
- [2] P. W. Higgs, Phys. Lett **12** (1964) 132, Phys. Rev. Lett. **13** (1964) 508; Phys. Rev. **145** (1966) 1156; F. Englert and R.Brout, Phys. Rev. Lett. **13** (1964) 321; G. S. Guralnik, C. R. Hagen and T. W. B. Kibble, Phys. Rev. Lett. **13** (1964) 585; T. W. B. Kibble, Phys. Rev. **155** (1967) 1554.
- [3] M. Carena, J.S. Conway, H.E. Haber, J.D. Hobbs, *et al.*, 'Report of the Tevatron Higgs working group', arXiv:hep-ph/0010338.
- [4] A. Stange, W.J. Marciano and S. Willenbrock, Phys. Rev. **D49**(1994) 1354, arXiv:hep-ph/9309294 and Phys. Rev. **D50**(1994)4491, arXiv:hep-ph/9404247.
- [5] ATLAS Collaboration, Technical Design Report, Vols. 1 and 2, CERN-LHCC-99-14 and CERN-LHCC-99-15; CMS Collaboration, Technical Proposal, CERN-LHCC-94-38; A. Djouadi *et al.*, 'The Higgs working group: Summary report', proceedings of the Workshop On Physics At TeV Colliders, Les Houches, France, 1999, arXiv:hep-ph/0002258; D. Cavalli

- et al.*, 'The Higgs working group: Summary report', proceedings of the Workshop On Physics At TeV Colliders, Les Houches, France, 2001, arXiv:hep-ph/0203056.
- [6] J.M. Butterworth, A.R. Davison, M. Rubin, G. P. Salam, Phys. Rev. Lett. **100** (2008) 242001, arXiv:0802.2470[hep-ph].
- [7] T. Han and S. Willenbrock, Phys. Lett. **B273**, 167 (1991); J. Ohnemus and W.J. Stirling, Phys. Rev. **D47** (1993) 2722; H. Baer, B. Bailey and J.F. Owens, Phys. Rev. **D47** (1993) 2730; S. Mrenna and C.P. Yuan, Phys. Lett. **B416** (1998) 200, arXiv:hep-ph/9703224; M. Spira, Fortsch. Phys. **46** (1998) 203, arXiv:hep-ph/9705337.
- [8] M. L. Ciccolini, S. Dittmaier, M. Krämer, Phys. Rev. **D68** (2003) 073003, arXiv:hep-ph/0306234v2.
- [9] O. Brein, A. Djouadi, R. Harlander, Phys. Lett. **B579** (2004)149, arXiv:hep-ph/0307206; O. Brein, M. Ciccolini, S. Dittmaier, A. Djouadi, R. Harlander, M. Krämer, 'Precision Calculations for Associated WH and ZH Production at Hadron Colliders', Contributed to 3rd Les Houches Workshop: Physics at TeV Colliders, arXiv:hep-ph/0402003v1.
- [10] J. Pumplin *et al.*, JHEP 0207, 012 (2002); D. Stump *et al.*, JHEP 0310, 046 (2003).
- [11] T. Hahn, Comput. Phys. Commun. **140** (2001)418.
- [12] T. Hahn, M. Perez-Victoria, Comput. Phys. Commun. **118** (1999)153.
- [13] S. Dittmaier, Nucl. Phys. **B675**(2003) 447; W. Beenakk, S. Dittmaier *et al.*, Nucl. Phys. **B653**(2003) 151.
- [14] G. Passarino and M. Veltman, Nucl. Phys. **B160** (1979) 151.
- [15] G.J. van Oldenborgh and J.A.M. Vermaseren, Z. Phys. **C46** (1990) 425.
- [16] B. W. Harris and J. F. Owens, Phys. Rev. **D65**, 094032(2002), hep-ph/0102128.
- [17] C. Amsler,*et al.* Phys. Lett. **B667**,1 (2008).

- [18] S.D. Ellis and D.E. Soper, Phys. Rev. **D48**,3160(1993), arXiv:hep-ph/9305266.
- [19] E. Boos, V. Bunichev, et al., (the CompHEP collaboration), Nucl. Instrum. Meth. **A534** (2004) 250-259, arXiv:hep-ph/0403113.
- [20] S. Dittmaier, S. Kallweit, P. Uwer, Phys. Rev. Lett. 100(2008) 062003; F. Campanario, C. Englert, M. Spannowsky, D. Zeppenfeld, Europhys. Lett. 88(2009)11001; T. Binoth, T. Gleisberg, S. Karg, N. Kauer, G sanguinetti, Phys. Lett. **B683**(2010) 154.